

Spin-waves in antiferromagnetic single crystal LiFePO_4

Jiying Li*, Vasile O. Garlea, Jerel L. Zarestky, and David Vaknin†

Ames Laboratory and Department of Physics and Astronomy, Iowa State University, Ames, IA 50011

(Dated: November 11, 2018)

Spin-wave dispersions in the antiferromagnetic state of single crystal LiFePO_4 were determined by inelastic neutron scattering measurements. The dispersion curves measured from the (010) reflection along both a^* and b^* reciprocal-space directions reflect the anisotropic coupling of the layered Fe^{2+} ($S = 2$) spin-system. The spin-wave dispersion curves were theoretically modeled using linear spin-wave theory by including in the spin-Hamiltonian in-plane nearest- and next-nearest-neighbor interactions (J_1 and J_2), inter-plane nearest-neighbor interactions (J_\perp) and a single-ion anisotropy (D). A weak (010) magnetic peak was observed in elastic neutron scattering studies of the same crystal indicating that the ground state of the staggered iron moments is not along (010) direction, as previously reported from polycrystalline samples studies, but slightly rotated away from this axis.

PACS numbers: 75.25.+z, 75.30.Ds, 75.50.Ee

I. INTRODUCTION

Lithium-orthophosphates LiMPO_4 ($M = \text{Mn, Fe, Co, Ni}$) have attracted a renewed interest in recent years, both for their relatively high lithium ionic-conductivity that can potentially be applied in rechargeable battery technology [1], and for their intriguing magnetic properties, in particular, the strong magneto-electric (ME) effect they exhibit [2]. In this regard, of particular importance is LiFePO_4 , as it has already been tested as a high-potential cathode in secondary Li-ion rechargeable battery [3, 4, 5, 6]. Like other members of the lithium-orthophosphates, LiFePO_4 is an insulator adopting the $Pnma$ space group [7, 8]. In this structure, the Fe^{2+} ion occupies the center of a slightly distorted MO_6 octahedron that shares oxygen anions with a PO_4 tetrahedron forming a closely packed oxygen framework. The Fe^{2+} ions ($S = 2$) form corrugated layers that are stacked along the [100] crystallographic axis, as shown in Fig. 1(a). Nearest neighbors in the b - c plane are coupled magnetically by a relatively strong exchange interaction, J_1 through an Fe-O-Fe oxygen-bond, whereas in-plane next-nearest-neighbors are coupled (J_2) via Fe-O-O-Fe [9] (see Fig. 1(b) for definition of exchange couplings). Interlayer magnetic coupling is mediated by a phosphate ion via an Fe-O-P-O-Fe bonding [10]. Thus, the olivine family of LiMPO_4 exhibits highly anisotropic properties which are between those of two- (2D) and three-dimensional (3D) systems [11, 12].

The magnetic properties of LiMPO_4 systems have been studied since the early 1960s [13, 14, 15]. They all undergo an antiferromagnetic transition at low temperatures to a similar magnetic arrangement differing only in the orientation of the staggered spins. Nearest-neighbor (NN) spins in the b - c plane are anti-parallel and the stacking along the a -axis is such that ferromagnetic

sheets perpendicular to the b -axis are formed; nearest neighbor sheets are anti-parallel giving rise to (010) fundamental magnetic reflection that, depending on the direction of the magnetic moment, can be intense or extinct. Earlier neutron diffraction studies of polycrystalline samples showed that the magnetic space group of LiFePO_4 and LiCoPO_4 is $Pnma'$ with the spins oriented along b crystallographic direction (i.e., the (010) reflection is absent), and $Pnm'a$ magnetic space group for LiNiPO_4 and LiMnPO_4 with the spins aligned parallel to the c -axis (i.e., strong intensity at the (010) reflection) [11, 12, 15, 16, 17, 18]. Recent neutron diffraction measurements of single crystal LiCoPO_4 reported finite intensity at the (010) reflection, interpreted in terms of a ground state with a spin direction that is slightly rotated from the b -axis [12]. Weak ferromagnetism has been reported for LiMnPO_4 [18] and LiNiPO_4 [19] at a temperature below T_N .

Recently, the magnetic structure and properties of lithium orthophosphates have been reexamined theoretically and experimentally [20, 21]. Rouse et al. [21] reported neutron diffraction results from polycrystalline samples confirming the collinear structure below $T_N = 52$ K. Magnetic properties of LiFePO_4 investigated by Mössbauer spectroscopy and magnetization measurement determined that $T_N = 50$ K [22]. Theoretical estimations of the spin exchange coupling by spin-dimer analysis, while neglecting the single ion-anisotropy, yield the following values $J_1 = 1.08$ meV, $J_2 = -0.4$ meV and $J_\perp = -0.92$ meV [9]. However, so far there has been no experimental determination of the exchange coupling among Fe^{2+} spins and of the single-ion anisotropy in LiFePO_4 , for comparison with the theoretical predictions. Knowledge of exchange couplings and single-ion-anisotropy is also important for understanding the origin of the strong magneto-electric (ME) effect in LiFePO_4 [13]. All lithium orthophosphates exhibit a strong yet anomalous linear magnetoelectric (ME) effect with respect to the observed ME tensor components, α_{xy} , α_{yx} , for LiFePO_4 and LiCoPO_4 , and α_{xz} , α_{zx} for LiNiPO_4 , as expected with their respective antiferromagnetic point

*electronic mail: jiy@ameslab.gov

†electronic mail: vaknin@ameslab.gov

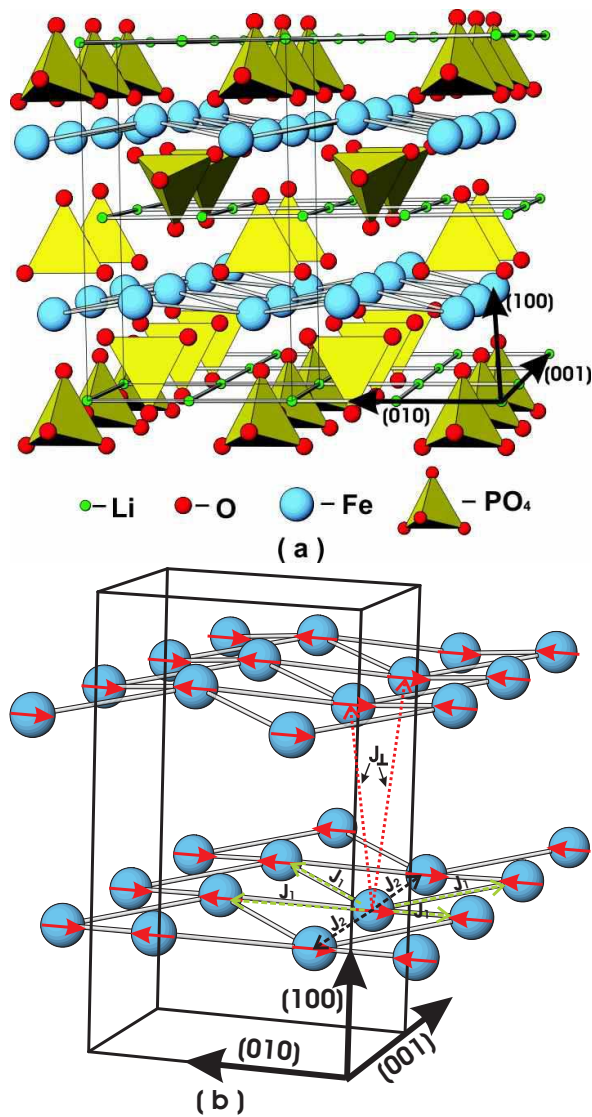


FIG. 1: (color online) (a) Atomic structure of LiFePO₄. The Fe²⁺ ions form buckled layers stacked perpendicular to the [100] crystallographic direction. The ground state of LiFePO₄ is collinear antiferromagnetic with the average moment along *b* direction. (b) Spin arrangement of the two Fe²⁺ layers, the in-plane nearest and next-nearest neighbor interactions J_1 and J_2 and inter-plane nearest neighbor inaction J_{\perp} are labeled.

groups mmm' and $mm'm$ [23, 24, 25, 26]. In particular, the ME effect measurements of LiFePO₄ as a function of temperature reveal a decrease of the ME coefficient along one direction $\alpha_{yx}(T)$ below a maximum close to T_N [23, 24]. Detailed determination of the magnetic structure using neutron diffraction from single crystals can shed light on the origin of these anomalies.

Herein, we report measurements of spin-wave dispersion curves of single crystal LiFePO₄ by inelastic neutron scattering measurements. Spin wave dispersion curves can provide the values of exchange interactions and the single ion anisotropy. The measured dispersion curves

were modeled using linear spin wave theory by including the in-plane nearest-neighbors (NN) and next-nearest-neighbors (NNN) spin couplings the inter-plane nearest-neighbor spin coupling and the single-ion anisotropy. We have also employed single-crystal elastic neutron diffraction techniques to investigate whether there are subtle deviations from the previously reported magnetic structure determined from neutron diffraction measurements of polycrystalline samples.

II. EXPERIMENTAL DETAILS

LiFePO₄ single crystals were grown by standard flux growth technique (LiCl was used as the flux) from a stoichiometric mixture of high purity FeCl₂ (99.999% Aldrich) and Li₃PO₄ (99.999% Aldrich) [27]. The grown single crystals have a dark greenish color. The composition and structure were confirmed by carrying out Rietveld analysis of the X-ray powder diffraction (XRD) data, using the GSAS software package [28]. No extra peaks from impurities were detected in the XRD pattern. Powder, for the XRD, was produced by crushing typical isolated single crystals from the melt. The lattice parameters yielded from the refinement ($a = 10.337$ Å, $b = 6.011$ Å, and $c = 4.695$ Å) are in good agreement with literature values [15, 20, 21].

Neutron scattering measurements were carried out on the HB1A triple axis spectrometer at High Flux Isotope Reactor at Oak Ridge National Laboratory. A monochromatic neutron beam of wavelength $\lambda = 2.366$ Å (14.6125 meV, $k_o = 2\pi/\lambda = 2.656$ Å⁻¹) was selected by a double monochromator system, using the (0 0 2) Bragg reflection of highly oriented pyrolytic graphite (HOPG) crystals. HOPG crystal was also used as analyzer for both the elastic and the inelastic studies. The $\lambda/2$ component in the beam was removed by two HOPG filters located before and after the second monochromator. The collimating configuration 40' - 40' - Sample - 34' - 68' was used throughout the experiments. Temperature measurements and control were achieved by a conducts LTC-20 using Lake Shore silicon-diode temperature sensors. An irregular shaped single crystal (weight ~ 0.4 g) was folded in aluminum foil and mounted on a thin aluminum post. It was then sealed in an aluminum can under helium atmosphere and loaded onto the tip of a closed-cycle helium refrigerator (Displex). Two temperature sensors were mounted on the cold-tip of the Displex and on the sample can. The temperature was controlled using the cold-tip sensor. The temperature difference between the two sensors was about 0.2 K over the temperature range investigated.

III. RESULTS AND DISCUSSION

A. Elastic neutron scattering

The LiFePO₄ crystal was oriented such that the *a-b* plane coincided with the horizontal scattering plane of the spectrometer. The elastic measurements confirmed that the magnetic structure of LiFePO₄ is antiferromagnetic with the main direction of the moment oriented along the *b*-axis. However, contrary to the previous neutron diffraction experiments performed on powder samples, we have detected the presence of the (0 1 0) reflection. The intensity of this peak is relatively weak but its intensity follows a similar temperature dependence as that of a stronger magnetic peak (210) (see Fig. 2). It is worth noting that the (0 1 0) peak is forbidden by the symmetry of the *Pnma'* magnetic space group previously proposed to describe the spin arrangement in LiFePO₄ [15, 20]. In the *Pmna* crystal symmetry, the point group of the Fe 4*c* site is *m_y* and the only allowable magnetic point groups are, therefore, *m_y* with the Fe magnetic moments along the *b*-axis (perpendicular to the mirror (010) plane) and *m'_y* with the magnetic moment lying in the mirror (010) plane. The magnetic contribution to the (010) peak indicates that the ordered moment is not strictly oriented along the *b*-axis and a small component perpendicular to this axis is present. This implies a lowering of the symmetry of the magnetic space group where both magnetic components (along and perpendicular to *b*-axis) are allowed. From the intensity ratio of the two reflections $I(010)/I(210)$ at low temperatures, we can estimate the angle of the staggered moment with respect to the *b*-axis, by using the following relation,

$$\frac{F_{(010)} \sin(\alpha_{(010)})}{F_{(210)} \sin(\alpha_{(210)})} = \sqrt{\frac{I_{(010)} \sin(2\theta_{(210)}) f_{(210)}}{I_{(210)} \sin(2\theta_{(010)}) f_{(010)}}} \quad (1)$$

where, $F_{(210)}$ and $F_{(010)}$ are the magnetic structure factors of peaks (210) and (010), $\alpha_{(210)}, \alpha_{(010)}$ are the angles between the scattering vector of reflections (210), (010) and the magnetic moment, and f_i are the corresponding form factors[12]. Using $f_{(210)}/f_{(010)} \approx 0.85$, we estimate the moments are rotated by 7.5 ± 0.5 deg toward *c*-axis or 3 ± 0.5 deg toward *a*-axis. The ratio between the magnetic and nuclear contributions to the peak intensities of reflections (I_{mag}/I_{nuc}) can be used to determine the average magnetic moment, μ from

$$\mu = \sqrt{\frac{I_{mag}}{I_{nuc}} \frac{|F_{nuc}|^2}{|F_{mag}|^2} \frac{1}{f^2(Q) \sin^2 \alpha}} \quad (2)$$

where for the reflection in question, F_{nuc} , and F_{mag} are the nuclear and magnetic structure factors, I_{nuc} and I_{mag} are the nuclear and magnetic intensities and $f(Q)$ is the magnetic form factor of Fe²⁺ at momentum transfer $Q = 2k_0 \sin \theta$. I_{mag} can be calculated from the peak intensity difference at temperatures above and below T_N . Using the peak intensities of (210) at 300 K and 10 K to

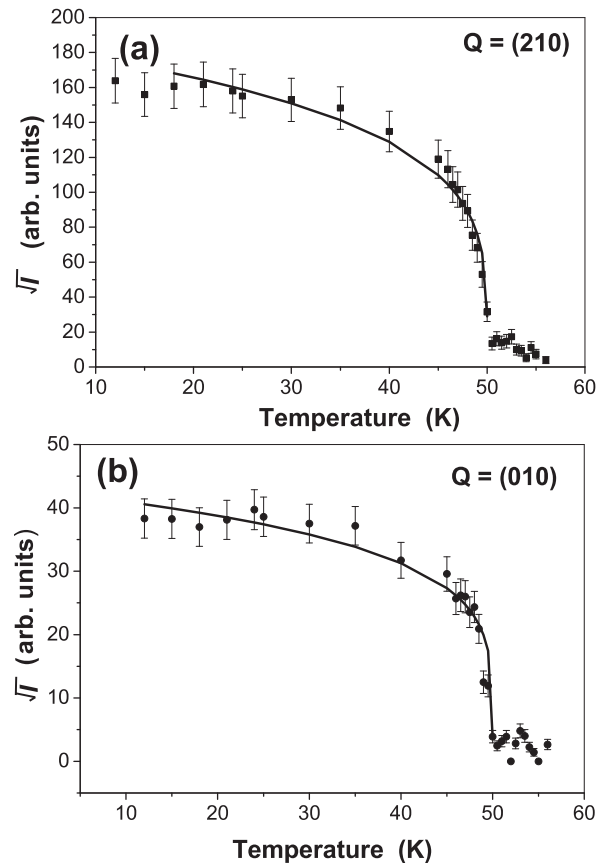


FIG. 2: Temperature dependence of the square root of the normalized integrated intensity at two reflection peaks (210) (a) and (010) (b). The transition temperature obtained from the fitting is $T_N = 50 \pm 0.5$ K and the critical exponent $\beta = 0.27 \pm 0.03$.

calculate the I_{mag} and I_{nuc} , and using $f_{(210)} = 0.85$, the calculated average magnetic moment μ for Fe is $3.93 \pm 0.05 \mu_B$, which is very close to the values of $3.99 \mu_B$ and $3.8 \mu_B$ obtained in Refs. [29] and [30].

To determine the temperature dependence of the order parameter, the (010) and (210) reflections were monitored as a function of temperature in the range 10 to 60 K. Figure 2(a) and (b) show the square root of the integrated intensity (\sqrt{I}) versus temperature. The \sqrt{I} quantity is proportional to the antiferromagnetic staggered magnetization, i.e., the order parameter. It was fitted to the following power law function near the transition temperature,

$$\sqrt{I} \propto M_0^\dagger = M_0^\dagger t^\beta \quad (3)$$

where, M_0^\dagger is the sub-lattice magnetization at $T = 0$ K, $t = (1 - T/T_N)$ is the reduced temperature, and β is the critical exponent. For the two magnetic peaks (010) and (210) the obtained transition temperatures are the same, $T_N = 50 \pm 0.5$ K and the critical exponent β is 0.27 ± 0.03 . The transition temperature is very close to the values reported in the literature 50 ± 2 K [15, 20, 22]. The

critical exponent β is slightly smaller than that calculated for the 3D Ising model ($\beta=0.32$) [31]. The temperature dependent background-like scattering above T_N and below ~ 60 K indicates some kind of critical scattering due to short-range order formation or due to a dimensionality cross-over.

B. Inelastic neutron scattering

The spin wave excitations were measured at 10 K along the $(\xi, 1, 0)$ and $(0, 1+\xi, 0)$ reciprocal space directions, for energy transfers (energy loss mode) ranging from 1 to 8.5 meV. As illustrated in Fig. 3 (a,b,c), well defined dispersive magnetic-modes of resolution-limited energy-width were observed at all wave vectors. A typical constant-q scan, performed at the zone center (010), is shown in Fig. 3 (a), indicating a single excitation at an energy transfer of 5.86 ± 0.04 meV. The increase in intensity at energy transfer below approximately 1 meV is due to the quasielastic scattering from the newly observed $(0, 1, 0)$ magnetic Bragg peak. Above the transition temperature ($T_N = 50$ K), at approximately 55 K, the inelastic peak at 5.86 meV disappears, confirming its magnetic origin. Such an energy gap in the dispersion curve is usually driven by single ion anisotropy. A similar energy gap of 2 meV at 2 K, was also observed in the LiNiPO_4 , and it was found to decrease with increasing the temperature [32]. In the case of LiFePO_4 , measurements performed at different temperatures indicate that the energy gap is temperature independent. The inelastic scattering signal measured at different constant wave-vectors ξ along the (100) and (010) reciprocal-space directions, at 10 K, are shown in Figure 3 (b, c). The data were fitted to Gaussian functions (solid line in Fig. 3 (a,b, c)) where the background was assumed to be constant.

The spin-wave dispersion branches deduced from these fits, for both b^* and a^* reciprocal-space directions, are plotted in Figure 4. It is shown that the dispersion curves monotonically increase in energy with ξ , and that the spin-waves propagating in the plane along the (010) direction have higher frequencies than those propagating transversally along the (100). Qualitatively, this behavior reflects the anisotropy in the strength of exchange couplings in the system; as expected the in-plane exchange couplings are much stronger than those between planes.

To construct a Hamiltonian for the spin system, we recall that in LiMPO_4 olivine family the in-plane super-exchange or super-super exchange interactions between nearest and next-nearest neighboring Fe^{2+} ions (J_1 and J_2) are expected to be much stronger than that between the nearest inter-plane neighbors (J_\perp) [10, 33]. Therefore, we propose the following Hamiltonian,

$$\mathcal{H} = -J_1 \sum_{i,\delta} (S_i S_{i+\delta}) - J_2 \sum_{i,\xi} (S_i S_{i+\xi}) - J_\perp \sum_{i,\delta_\perp} (S_i S_{\delta_\perp}) + D \sum_i (S^z)^2 \quad (4)$$

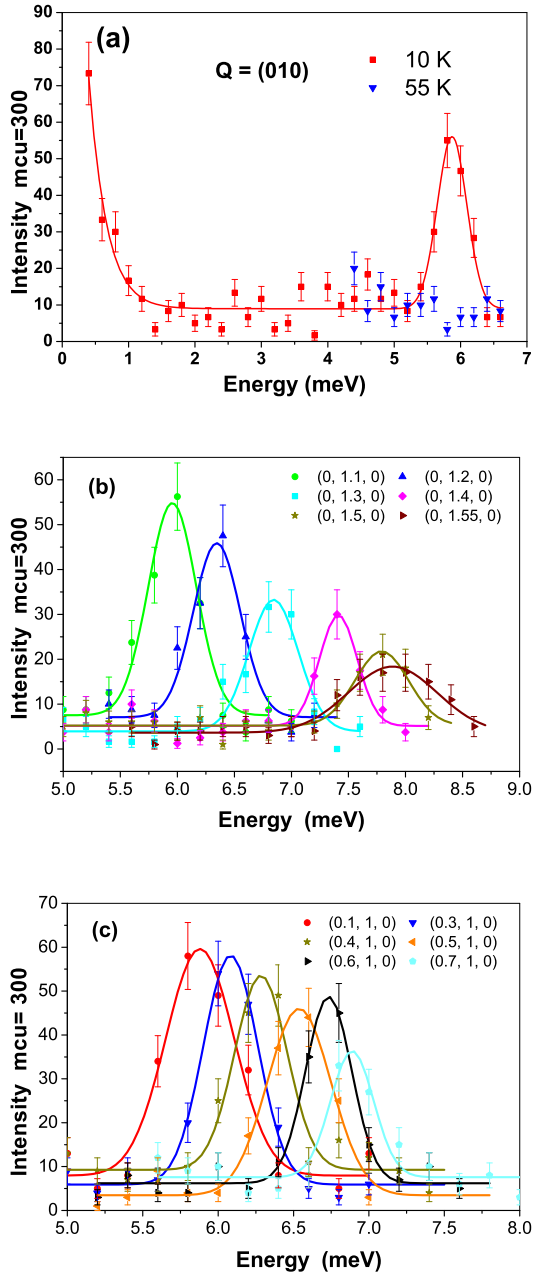


FIG. 3: (color online) (a) Neutron scattering intensity as a function of the energy transfer E at (010) peak at 10 K and 55 K. (b) Constant-Q scans taken at 10K, at different wave-vectors $(0, 1+\xi, 0)$ and (c) Constant-Q scans at $(\xi, 1, 0)$.

where, J_1 and J_2 are the in-plane NN and NNN coupling constants, respectively, and J_\perp is the inter-plane NN coupling constant. The illustrations of J_1 , J_2 and J_\perp are shown in Figure 1(b). D is the single-ion anisotropy constant quantifying the tendency of the spins to align along the easy axis (the S^z component is defined to be along the direction of the moment at the ground state - b^*). The Ising like ground state of the system is be-

lied to be invoked by the single-ion anisotropy term which comes about from crystal field effects and spin-orbit coupling [34]. Using the antiferromagnetic spin-wave theory[35, 36], the lattice with N sites was divided into two sublattices A and B, where nearest-neighbors of an Fe^{2+} site in one sub-lattice are all sites in the other sublattice. The next-nearest neighbors of an Fe^{2+} site are in the same sublattice. The magnon dispersion curves were calculated using the Holstein-Primakoff spin operator transformation to linear approximation (i.e., linear spin-wave theory [37]). The resulting spin-wave dispersion is given by

$$\hbar\omega = \sqrt{A^2 - F^2} \quad (5)$$

where $A = (2J_1ZS - 2J_2ZS - 2J_\perp ZS + 2J_2ZS\gamma_{3N} + 2J_\perp ZS\gamma_\perp + 2DS)$ and $F = 2J_1ZS\gamma_{2N}$, in which Z is the number of the nearest neighbors $Z = 4$, $S = 2$ for Fe^{2+} . γ_{2N} , γ_{3N} and γ_\perp are calculated using the following equation:

$$\gamma_{(2N,3N,\perp)} = \frac{1}{Z} \sum_i e^{i\mathbf{Q}\cdot\mathbf{r}} \quad (6)$$

where $\mathbf{r} = (\delta, \xi, \delta_\perp)$ are the components of vectors to the intra-plane nearest, next-nearest neighbors and to the inter-plane nearest-neighbor. We get

$$\gamma_{2N} = \cos(\pi k_y) \cos(\pi k_z) \quad (7)$$

$$\gamma_{3N} = \frac{1}{2}(\cos(2\pi k_y) + \cos(2\pi k_z)) \quad (8)$$

$$\gamma_\perp = \cos(\pi k_x) \cos(\pi k_y) \quad (9)$$

The experimental data along the $(0, 1+\delta, 0)$ and $(\delta, 1, 0)$ directions in Fig. 4 were fitted to Eq. (5) yielding the following values: $J_1 = -0.662 \pm 0.02$ meV, $J_2 = -0.27 \pm 0.02$ meV, $J_\perp = 0.021 \pm 0.001$ meV and $D = -0.37 \pm 0.01$ meV.

The in-plane nearest- and next-nearest-neighbor coupling constants quantitatively agree with theoretical calculations[9], $J_1 = -1.08$ meV and $J_2 = -0.4$ meV [9]. The two spin couplings, $J_1 < 0$ and $J_2 < 0$, compete oppositely over the alignment of in-plane NNN spins; whereas J_1 leads to parallel alignment of NNN spins J_2 favors their antiparallel alignment. Such competing interactions can lead to incommensurate phases[38] which were not found in this system. However, incommensurate phases have been reported for the isostructural LiNiPO_4 [26]. The inter-plane coupling $J_\perp = 0.021$ meV determined in this study is significantly smaller than the theoretical one $J_\perp = -0.92$ meV [9]. It should be noted that single-ion anisotropy was not considered in the theoretical calculations [9].

To summarize, we have measured spin-wave dispersions and determined spin exchange couplings in

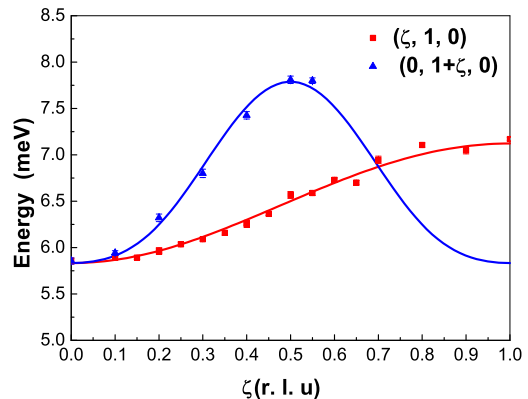


FIG. 4: (color online) Spin-wave dispersion curves along the b^* and a^* reciprocal space directions. Solid lines are fits obtained from Linear Spin-wave Theory using Eq(5).

LiFePO_4 . Our results show that although there are competing interactions between NN and NNN spins in LiFePO_4 , they do not lead to more complicated, incommensurate or non-collinear, magnetic structures. This is in contrast to the observation of incommensurate magnetic phases in LiNiPO_4 [26]. These competing interactions may explain the observation of weak-ferromagnetism in LiMPO_4 systems[18]. They may also be related to the observation, in this study, that the staggered magnetic moment is not aligned along a principal direction. From the gap in the spin wave dispersion curve, we have been able to extract the single-ion anisotropy in LiFePO_4 using linear spin-wave theory.

Acknowledgments

We thank R. J. McQueeney, S. Chang, and J. Q. Yan at Ames Laboratory for the helpful discussions. This work was supported (in part) under the auspices of the United States Department of Energy. The HFIR Center for Neutron Scattering is a national user facility funded by the United States Department of Energy, Office of Basic Energy Sciences- Materials Science, under Contract No. DE-AC05-00OR22725 with UT-Battelle, LLC. The work was supported by the Department of Energy, Office of Basic Energy Sciences under contract number W-7405-Eng-82.

-
- [1] J. -M. Tarascon, M. Armand, *Nature Mater.* **414**, 359 (2001).
- [2] M. Fiebig, *J. Phys. D: Appl. Phys.* **38**, R123 (2005).
- [3] A. K. Padhi, K. S. Nanjundaswamy, and J. B. Goodenough, *J. Electrochem. Soc.* **144**, 1188 (1997).
- [4] S. Y. Chung, J. T. Bloking, Y. M. Chiang, *Nature Mater.* **1**, 123 (2002).
- [5] P. S. Herle, B. Ellis, N. Coombs, A. F. Nazar, *Nature Mater.* **3**, 147 (2004).
- [6] C. Delacourt, P. Poizot, J. M. Tarascon, C. Masquelier, *Nature Mater.* **4**, 254 (2005).
- [7] S. Geller and J. L. Easson, *Acta Crystallogr.* **18**, 258 (1960).
- [8] H. D. Megaw, *Crystal Structures - A Working Approach*, Saunders, Philadelphia, 1973, P249.
- [9] D. Dai, M. H. Whangbo, H. J. Koo, X. Rocquefelte, S. Jobic, A. Villesuzanne, *Inorganic Chem.* **44**, 2407 (2005).
- [10] J. M. Mays, *Phys. Rev.* **131**, **38** (1963).
- [11] D. Vaknin, J. L. Zarestky, J. E. Ostenson, B. C. Chakoumakos, A. Goñi, P. J. Pagliuso, T. Rojo, and G. E. Barberis, *Phys. Rev. B* **60**, 1100 (1999).
- [12] D. Vaknin, J. L. Zarestky, L. L. Miller, J. -P. Rivera, and H. Schmid, *Phys. Rev. B* **65**, 224414 (2002).
- [13] M. Mercier, J. Gareyte, and E. F. Bertaut, *C. R. Seances, Acad. Sci. Ser. B* **264**, 979 (1967).
- [14] R. P. Santoro, D. J. Segal, and R. E. Newnham, *J. Phys. Chem. Solids* **27**, 1192 (1966).
- [15] R. P. Santoro and R. E. Newnham, *Acta Crystallogr.* **22**, 344 (1967).
- [16] A. Goñi, L. Lezama, G. E. Barberis, J. L. Pizarro, M. I. Arriortua and T. Rojo, *J. Mag. Mag. Mater.* **164**, 251 (1996).
- [17] D. Arçon, A. Zorko, R. Dominko, Z. Jaglicic, *J. Phys. Chem. Solids* **16**, 5531 (2004).
- [18] Y. Kharchenko, N. Kharchenko, M. Baran and R. Szymczak, *Low Temp. Phys.* **29**, 579 (2003).
- [19] D. Arçon, A. Zorko, P. Cevc, R. Dominiko, M. Bele, J. Jamnik, Z. Jaglicic, I. Golosocsky, *J. Phys. Chem. Solids*, **65** 1773 (2004).
- [20] V. A. Streltsov, E. L. Belokoneva, V. G. Tsirelson and N. K. Hansen, *Acta Crystal.* **B49**, 147 (1993).
- [21] G. Rousse, J R. Carvajal, S. Patoux and C. Masquelier, *Chem. Mater.* **15**, 4082 (2003).
- [22] Luo Zhi, Di Nai-Li, Kou Zhi-Qi, Cheng Zhao-Hua, Liu Li-Jun, Chen Li-Quan, and Huang Xue-Jie, *Chinese Phys.* **13**, 2158 (2004).
- [23] M. Mercier, P. Bauer, *C. R. Acad. Sci. Paris* **267**, 465 (1968).
- [24] M. Mercier, *Rev. Gen. Electr.* **80**, 143 (1971).
- [25] J. -P. Rivera, *Ferroelectrics* **161**, 147 (1994).
- [26] D. Vaknin, J. L. Zarestky, J. -P. Rivera, and H. Schmid, *Phys. Rev. Lett.* **92**, 207201 (2004).
- [27] V. I. Fomin, V. P. Genezdilov, V. S. Kurnosov, A. V. Peschanski, A. V. Yeremenko, H. Schmid, J. -P. Rivera, and S. Gentil, *Low Temp. Phys.* **28**, 203 (2002).
- [28] A. C. Larson, R. B. Von Dreele, and M. Lujan Jr., *Computer code GSAS, Generalized Structure Analysis System*, Neutron Scattering Center, Los Alamos National Laboratory, (1990).
- [29] Y. N. Xu, S. Y. Chung, J. T. Bloking, Y. M. Chiang, and W. Y. Ching, *Electrochem. Solid-State Lett.* **7**, A131 (2004).
- [30] A. Yamada, S. C. chung, and K. Hinokuma, *J. Electrochem. Soc.* **148**, A224 (2001).
- [31] M. F. Collins, *Magnetic Critical Scattering*, New York, Oxford University Press, 1989, p29.
- [32] J. Li, *et. al.*, to be published.
- [33] S. Shi, C. Y. Quyang, Z. H. Xiong, L. J. Liu, Z. X. Wang, H. Li, D. S. Wang, L. Q. Chen, and X. J. Huan, *Phys. Rev. B* **71**, 144404 (2005).
- [34] L. J. de Jongh, in *Magnetic Properties of Layered Transition Metal Compounds*, Kluwer Academic, Dordrecht, 1990. P. 1.
- [35] P. W. Anderson, *Phys. Rev.* **86**, 694 (1952).
- [36] R. Kubo, *Phys. Rev.* **87**, 568 (1952).
- [37] G. L. Squires, in *Introduction to the Theory of Thermal Neutron Scattering*, Cambridge University Press, New York, 1978, P156.
- [38] P. Bak, *Rep. Prog. Phys.* **45**, 687 (1982).